

Hyperspectral and LiDAR Data Fusion: Outcome of the 2013 GRSS Data Fusion Contest

Christian Debes, *Senior Member, IEEE*, Andreas Merentitis, *Member, IEEE*, Roel Heremans, Jürgen Hahn, *Student Member, IEEE*, Nikolaos Frangiadakis, *Member, IEEE*, Tim van Kasteren, Wenzhi Liao, *Member, IEEE*, Rik Bellens, *Member, IEEE*, Aleksandra Pižurica, *Member, IEEE*, Sidharta Gautama, *Member, IEEE*, Wilfried Philips, *Senior Member, IEEE*, Saurabh Prasad, *Member, IEEE*, Qian Du, *Senior Member, IEEE*, and Fabio Pacifici, *Senior Member, IEEE*

Abstract—The 2013 Data Fusion Contest organized by the Data Fusion Technical Committee (DFTC) of the IEEE Geoscience and Remote Sensing Society aimed at investigating the synergistic use of hyperspectral and Light Detection And Ranging (LiDAR) data. The data sets distributed to the participants during the Contest, a hyperspectral imagery and the corresponding LiDAR-derived digital surface model (DSM), were acquired by the NSF-funded Center for Airborne Laser Mapping over the University of Houston campus and its neighboring area in the summer of 2012. This paper highlights the two awarded research contributions, which investigated different approaches for the fusion of hyperspectral and LiDAR data, including a combined unsupervised and supervised classification scheme, and a graph-based method for the fusion of spectral, spatial, and elevation information.

Index Terms—Data fusion, hyperspectral, Light Detection And Ranging (LiDAR), multi-modal, urban, VHR imagery.

I. INTRODUCTION

NOWADAYS, diverse sensor technologies allow to measure different aspects of objects on the Earth, from spectral characteristics in multispectral and hyperspectral images (HSIs), to height information in Light Detection And Ranging (LiDAR) data, to amplitude and phase in synthetic aperture radar (SAR) systems. Despite the richness of information available, automatic interpretation of remote sensed data is still very difficult.

Individually, the use of hyperspectral imagery and LiDAR data has been an active research focus in the community. The passive sensing of hyperspectral systems can be effective in describing the phenomenology of the observed scene over a continuum of spectral channels, whereas the active sensing of LiDAR systems can be exploited for characterizing topographical information of

the scene. Unlike hyperspectral sensing, LiDAR data can be acquired at any time of the day and under different weather conditions. In recent years, various techniques have been developed for effective feature extraction (FE), feature selection, semi-supervised, active learning, and ensemble classification of hyperspectral imagery [1]–[11]. Likewise, the LiDAR community has been very active in developing techniques for extracting features from the raw data for various applications [12]–[15].

However, it is obvious that no single technology can be always sufficient for reliable image interpretation [16]. For example, hyperspectral imagery should not be used to differentiate objects composed of the same material, such as roofs and roads both made of concrete. On the other hand, LiDAR data alone cannot be used to separate objects with the same elevation, such as roads with the same height but made of asphalt or concrete. The data fusion problem has been addressed in the literature, recommending best-practices about using data from different sources. However, combining too many features may lead to the problem of the curse of dimensionality and excessive computation time [17]. Feature reduction techniques are often used to mitigate such a problem [2], [16, 18, 19]. In addition, decision fusion, as one type of data fusion, may present difficulties with modeling correlations between the different data sources [20].

The Data Fusion Technical Committee (DFTC) of the IEEE Geoscience and Remote Sensing Society (GRSS) serves as a global, multi-disciplinary, network for geospatial data fusion, with the objective of connecting people and resources, educating students and professionals, and promoting the best-practices in data fusion applications. The committee organizes an annual Data Fusion Contest open to the broader community with the goal of encouraging new techniques (and evaluating existing ones) for remote sensing problems using data from different sources [21]–[25].

The 2013 Data Fusion Contest was designed to investigate the synergistic use of hyperspectral and LiDAR data. More than 900 researchers from universities, national labs, space agencies, and corporations across the globe registered to the Contest, with the data sets being downloaded from a total of 69 different countries (with a large number of registrations from underdeveloped areas), demonstrating the great interest of the community in the DFTC activities. The 2013 Data Fusion Contest consisted of two parallel competitions

- 1) *Best Classification Challenge*: to promote innovation in classification algorithms, and to provide objective and fair

Manuscript received October 25, 2013; revised January 04, 2014; accepted January 31, 2014. This work was supported in part by the IEEE Geoscience and Remote Sensing Society, DigitalGlobe, Inc. and in part by the SBO-IWT project Chameleon (Domain-specific Hyperspectral Imaging Systems for Relevant Industrial Applications).

C. Debes, A. Merentitis, R. Heremans, N. Frangiadakis, and T. van Kasteren are with AGT International, 64295 Darmstadt, Germany.

W. Liao, R. Bellens, A. Pižurica, S. Gautama, and W. Philips are with the Ghent University-iMinds, 9000 Ghent, Belgium.

J. Hahn is with the Technische Universität Darmstadt, 64283 Darmstadt, Germany.

S. Prasad is with the University of Houston, Houston, TX 77004 USA.

Q. Du is with the Mississippi State University, Mississippi State, MS 39762 USA.

F. Pacifici is with DigitalGlobe Inc., Longmont, CO 80503 USA.

Color versions of one or more of the figures in this paper are available online at <http://ieeexplore.ieee.org>.

Digital Object Identifier 10.1109/JSTARS.2014.2305441

performance comparisons among state-of-the-art algorithms. For this task, users were asked to submit a classification map of the data using the training samples generated by the DFTEC via photo-interpretation. The validation set was kept unknown to the participants.

- 2) *Best Paper Challenge*: with the objective of promoting novel synergistic use of hyperspectral and LiDAR data. The deliverable was a 4-page manuscript that addressed the problem, methodology, and results. Participants were encouraged to consider various open problems on multi-sensor data fusion, and to use the provided data set to demonstrate novel and effective approaches to solve these problems.

After rigorous review by the Data Fusion Award Committee, two winning submissions were selected (one per challenge), and their authors were awarded IEEE GRSS Certificates of Appreciation during the 2013 IEEE International Geoscience and Remote Sensing Symposium (IGARSS) held in Melbourne, Australia.






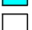






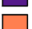


This paper highlights the two awarded research contributions. It is organized as follows: Section II addresses a brief literature review on the fusion of hyperspectral and LiDAR data, whereas the data sets are introduced in Section III. The contributions by the two winning teams are then described in detail. Specifically, Section IV describes a two-stream classification framework proposed by Debes, Merentitis, Heremans, Hahn, Frangiadakis, and van Kasteren, in which the hyperspectral and LiDAR data are combined by a parallel process that involves both unsupervised and supervised classification. Section V presents a methodology for the fusion of spectral, spatial, and elevation information by a graph-based approach proposed by Liao, Bellens, Pižurica, Gautama, and Philips. Finally, conclusions and perspectives drawn from this Contest are discussed in Section VI.

II. LITERATURE REVIEW

Due to the increased availability of hyperspectral and LiDAR data taken from the same area, the fusion of these remote sensing data has been of great interest for many practical applications. Elakshe [26] fused hyperspectral and LiDAR data for coastal mapping by using hyperspectral imagery to discriminate road and water pixels, and LiDAR data to detect and create a vector layer of building polygons. In [27], Swatantrana *et al.* explored fusion of structural metrics from the LiDAR data and spectral characteristics from the hyperspectral imagery for biomass estimation in the Sierra Nevada. Shimoni *et al.* [28] used a score-level fusion approach for detecting stationary vehicles under shadows, where detection scores from both hyperspectral and LiDAR data are derived separately and combined with a simple sum rule. By fusing LiDAR and hyperspectral data through a physical model, Zhang *et al.* [29] developed a simple but efficient illumination correction method to remove the direct illumination component of the observed hyperspectral radiance data, and detected objects under shadows.

For mapping-related applications, the approach in [30] explored the joint use of hyperspectral and LiDAR data for the separation of vegetation classes, underlining that LiDAR can be very useful in the separation of shrubs from trees. Lemp and Weidner [31] exploited hyperspectral and LiDAR data for the classification of urban areas, using LiDAR for the segmentation

TABLE I
CLASSES, TRAINING AND VALIDATION SAMPLES, AND COLOR CODE

Class name	Training set	Test set	Class color
Healthy grass	198	1053	
Stressed grass	190	1064	
Synthetic grass	192	505	
Tree	188	1056	
Soil	186	1056	
Water	182	143	
Residential	196	1072	
Commercial	191	1053	
Road	193	1059	
Highway	191	1036	
Railway	181	1054	
Parking lot 1	192	1041	
Parking lot 2	184	285	
Tennis court	181	247	
Running track	187	473	

of the scene, and then hyperspectral information for the classification of the resulting regions. In [32], Mundt *et al.* fused co-registered LiDAR and hyperspectral data to map sagebrush communities and suggested further use of classified vegetation maps in biomass calculations. Sugumaran and Voss addressed the joint use of hyperspectral and LiDAR data for the identification of tree species in an urban environment [33], showing the effectiveness of LiDAR in the classification phase. Koetz *et al.* classified fuel composition from fused LiDAR and hyperspectral bands using Support Vector Machines (SVM) [34], demonstrating that the classification accuracies from fusion were higher than from either sensor alone. The joint use of hyperspectral and LiDAR remote sensing data for the classification of forests was investigated in [35], where a novel classification system was proposed to properly integrate multi-sensor information. The approach in [36] merged point cloud LiDAR data and hyperspectral imagery into a single sparse modeling pipeline for subpixel mapping and classification. Naidoo *et al.* [37] classified eight common savanna tree species in the Greater Kruger National Park region, South Africa, by fusing hyperspectral and LiDAR data in an automated Random Forest modeling approach. The recent work in [38] applied extended morphological attribute profiles (EAPs) [39] to both hyperspectral and LiDAR data for classification tasks, where the EAP features were extracted from both hyperspectral and LiDAR data, and used together with spectral, spatial, and elevation information in a stacked structure. Some limitations in stacking different morphological attributes were discussed by Dalla Mura *et al.* in [40].

III. DATA SET

The data sets distributed for the Contest included an HSI, a LiDAR-derived digital surface model (DSM), both at the same spatial resolution (2.5 m), as well as the LiDAR point cloud. The HSI had 144 bands in the 380–1050 nm spectral region. The corresponding co-registered DSM represented the elevation in meters above sea level (per the Geoid 2012 A model). The “las” file of the LiDAR point cloud was also provided. The data sets were acquired by the NSF-funded Center for Airborne Laser Mapping (NCALM) over the University of Houston campus and its neighboring area. The LiDAR data was acquired on June 22,

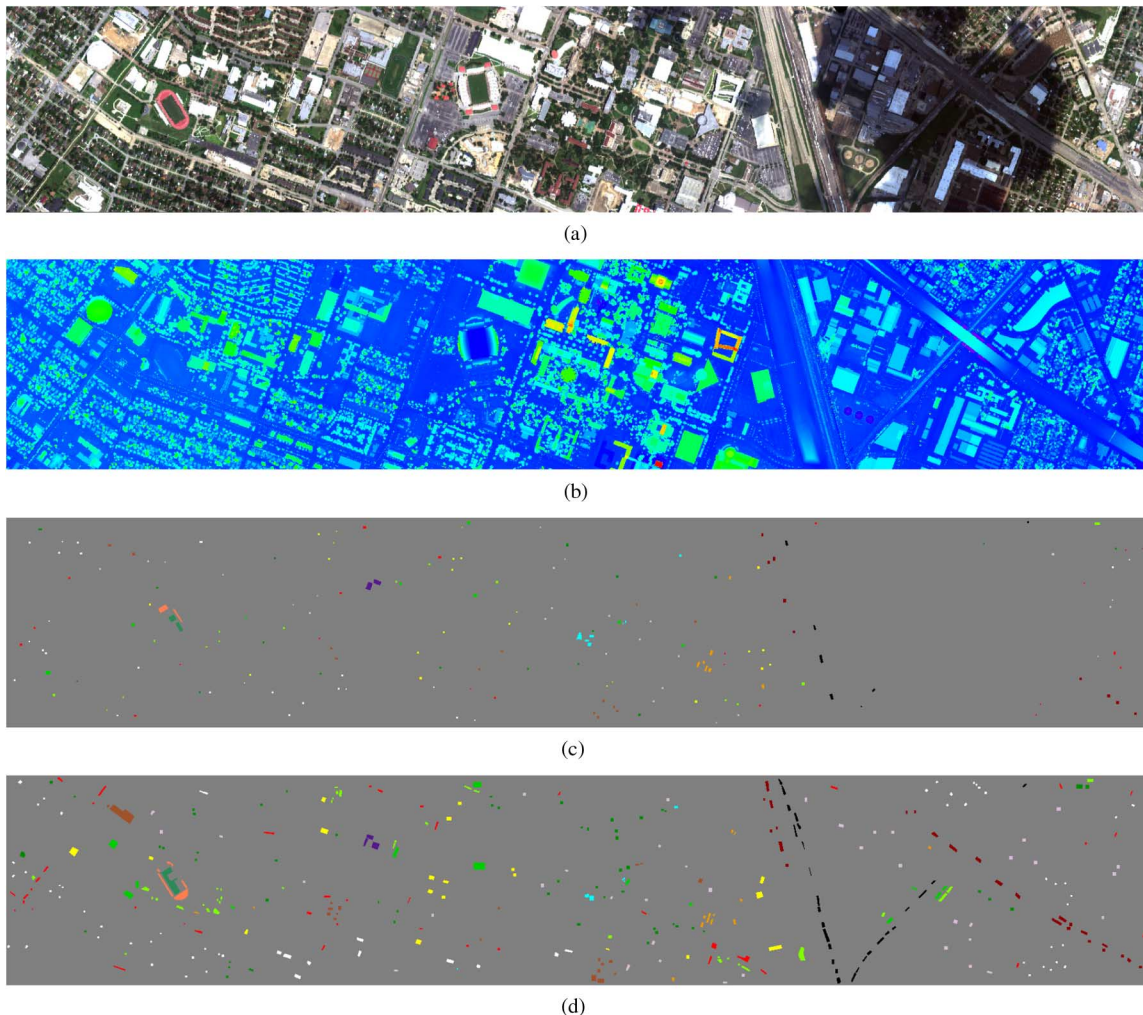


Fig. 1. Data sets used in the Contest: (a) HSI, (b) the LiDAR-derived DSM, and the location of the (c) training, and (d) validation samples. Color code is reported in Table I.

2012, between 14:37:55 and 15:38:10 UTC. The average height of the sensor above ground was 2000 feet. The HSI was acquired on June 23, 2012 between 17:37:10 and 17:39:50 UTC. The average height of the sensor above ground was 5500 feet.

The 15 classes of interest selected by the DFTC are reported in Table I with the corresponding number of samples for both the training and the validation sets. As shown, both land cover and land use classes were considered, including natural objects (e.g., grass, tree, soil, and water), and man-made objects (e.g., road, highway, and railway). Note that the “Parking Lot 1” class included parking garages at ground level and in elevated areas, and “Parking Lot 2” corresponded to parked vehicles. For each class, the size of training and validation sets was made constant (when possible) to include about 200 and 1000 samples, respectively. Fig. 1 shows the HSI, the LiDAR-derived DSM, and the locations of the training and validation samples. It is noteworthy that a large cloud shadow was present during the acquisition of the HSI; as a result, no training samples were selected in this region. However, a significant number of validation samples was collected to test the efficacy of various algorithms in dealing with cloud shadow. As mentioned earlier, the validation set was not distributed to the participants.

IV. TWO-STREAM FUSION FRAMEWORK FOR HYPERSPECTRAL AND LIDAR IMAGERY

This section describes a classification framework for the fusion of hyperspectral and LiDAR data. As shown in Fig. 2, the unsupervised and supervised classification approaches are run in parallel. The aim of the “Unsupervised Object Detection” module is to extract candidate objects (such as buildings or streets) in an unsupervised fashion. These objects support the “Supervised Classification” module, which consists of two components: “FE” and “classification based on ensemble learning”. Successively, the results of the two branches are fused in the “Object-based classification and correction” module to produce the final classification map.

A. Proposed Method

1) *Unsupervised Object Detection*: Given the registered HSI and the LiDAR-derived elevation map, the first step in the “Unsupervised Object Detection” module is to extract features representing the spatial distribution that is of relevance for object extraction. In the following examples, the vegetation index and elevation were selected as features. For example, pixels that

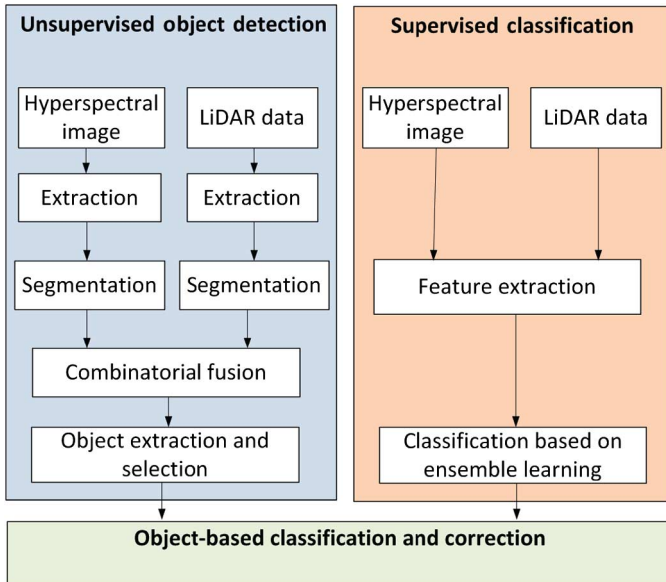


Fig. 2. Proposed data fusion framework.

represent a commercial building would necessarily have low vegetation index values and high elevation.

Each of these features y^g is segmented to obtain a binary map x^g , with $g = 0, \dots, G - 1$ and G being the number of features, where a binary “1” denotes the presence of the feature (e.g., “vegetation”) and a binary “0” denotes its absence (e.g., “no vegetation”). Neighborhood relations are taken into account by using a Markov Random Field (MRF)-based approach, namely the ICM algorithm [41], [42], that iteratively maximizes the posterior as

$$\hat{x}^g = \underset{x^g}{\operatorname{argmax}} \{p(x^g)p(y^g|x^g)\} \quad (1)$$

and it has been successfully applied in many applications of remote sensing [43], [44].

Successively, the segmented binary maps x^g are merged by multiplying all combinations of the binary maps x^g for their respective counterparts $(1 - x^g)$. This yields a total of 2^G binary maps containing all the possible combinations. Table II illustrates the case of two features ($G = 2$), i.e., a vegetation index derived from the HSI and the elevation information derived from LiDAR data. In this case, the respective segmentation maps x^0 and x^1 can be fused in four different ways.

The obtained binary maps contain contiguous pixels sets that have similar characteristics. These sets are considered as candidate objects in the “Object extraction and selection” module. This step is performed to remove outliers. Three cluster types are discussed in the following as example:

- 1) *Commercial buildings*: the combination of “low vegetation” and “high elevation” is considered for this cluster. The selection is based on the object area and solidity (the ratio of the pixel area and the convex hull around the object), as commercial buildings typically have large area occupancy and high solidity. Fig. 3(a) and (b) illustrates an example of selecting objects according to this rule, where all objects with area smaller than 3000 m^2 (approximately 480 pixels) and solidity less than 0.75 are removed.

TABLE II

THE FOUR FUSION MAPS BASED ON THE COMBINATIONS OF VEGETATION AND ELEVATION INFORMATION

Operation	Feature	Cluster
$x^0 \cdot x^1$	High veg, high elev	Trees
$x^0 \cdot (1 - x^1)$	High veg, low elev	Grass
$(1 - x^0) \cdot x^1$	Low veg, high elev	Buildings
$(1 - x^0) \cdot (1 - x^1)$	Low veg, low elev	Streets

- 2) *Parking lots*: the combination of “low vegetation” and “low elevation” is considered for this cluster. In order to remove street pixels, the width of each object is estimated using morphological operations, where all objects with a width smaller than 10 m are discarded. Region growing is applied to the remaining objects to estimate the occupied area A . The differences of the farthest and closest positions covered by the object are considered as the length l_u and width w_u of each object, similarly to an axis-aligned bounding box. Based on l_u and w_u , two features are derived, the side aspect ratio

$$R_{\text{aspect}} = \frac{w_u}{l_u} \quad (2)$$

and the coverage ratio

$$R_{\text{coverage}} = \frac{A}{l_u \cdot w_u}. \quad (3)$$

The coverage ratio measures the similarity of the size of the bounding box and the area of the object. Since the bounding box can be considered as a completely dense object (i.e., without any gaps), this feature provides information about object density. Finally, the parking lots are filtered by thresholding. In the example, in Fig. 3(c) and (d), R_{coverage} was set to 0.4 to make sure that the object is dense. Further, it was assumed that a parking lot covers an area of at least $A > 50 \text{ m}^2$ (approximately 8 pixels), with the side aspect ratio R_{aspect} between 1/3 and 3 to remove long and relatively thin objects such as highway or railway.

- 3) *Streets*: the combination of “low vegetation” and “low elevation” is considered for this cluster. From a large number of candidates, a subset of objects is selected by removing the previously found parking lots. This segmentation map is referred to as *street segmentation map*. The remaining candidate street objects are consequently skeletonized as shown in Fig. 3(e). Using the Hough transform on the binary skeleton [45], a selection of Hough lines is retrieved based on the highest Hough peaks. The high Hough peaks corresponding to short line segments are discarded and only the longest line segments are retained. In the next step, the line segments are grown laterally until the width for which up to 80% of additional pixels in the rectangle are classified as low vegetation and low elevation pixels in the *street segmentation map*. The result of this operation is shown in Fig. 3(f).

2) *Supervised Classification*: The output of the “Unsupervised Object Detection” module is not the final classification map, but rather an initial clustering of candidate objects. The “Supervised classification” represents the right branch of the framework

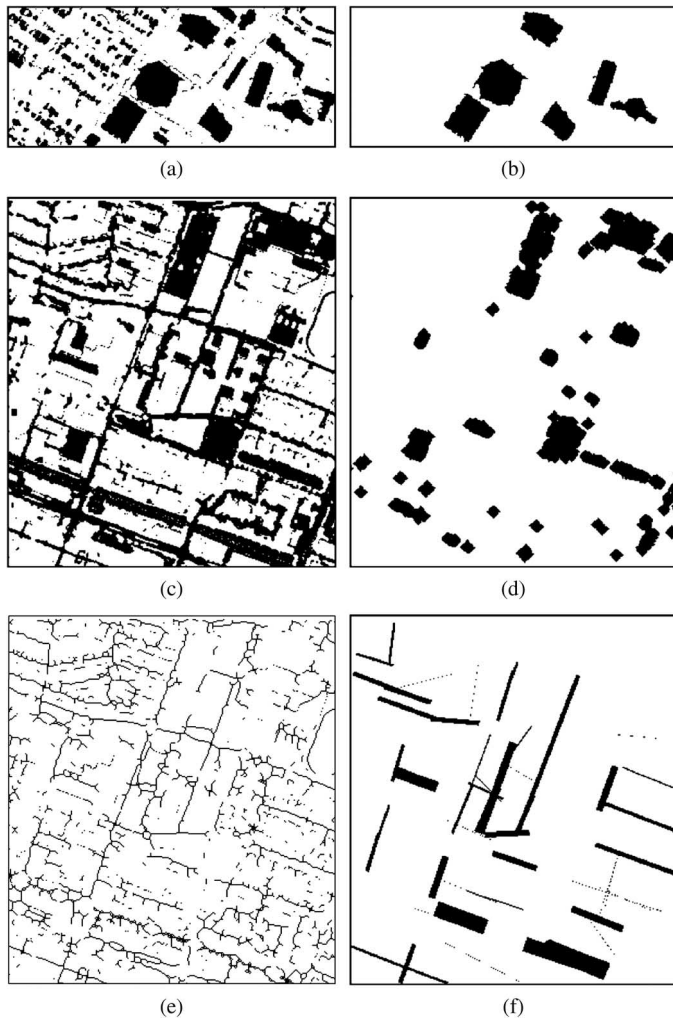


Fig. 3. Combination maps for (a) low vegetation/high height, and (b) extracted commercial buildings, (c) low vegetation/low elevation, (d) extracted parking lots, (e) street skeletons, and (f) streets.

illustrated in Fig. 2, and it is composed by the “FE” and “classification based on ensemble learning” steps. The “FE” module applies blind unmixing using Automatic Target Generation Procedure [46] to extract endmembers. In total, 50 basic endmembers are automatically extracted and their abundance maps are used as features for the pixel-based classification. Since the list of materials identified by the extraction of abundance maps might not be exhaustive (especially in the more challenging shadow-covered part of the image), Minimum Noise Fraction (MNF) transform [47] is also applied on the original spectral bands to preserve the information that might not get extracted from the abundance maps. Moreover, composite features of the hyperspectral data, such as vegetation index and water vapor absorption, are considered, because they are particularly helpful in discriminating vegetation and water bodies, respectively. Finally, the raw LiDAR-derived elevation map and composite topology features (such as gradients) are used to further increase the classification accuracy.

It is worth mentioning that the abundance features, when combined with the LiDAR information, are very effective as shown in Fig. 4, which illustrates the impact of adding LiDAR information to the extracted 50 abundance maps, compared to the

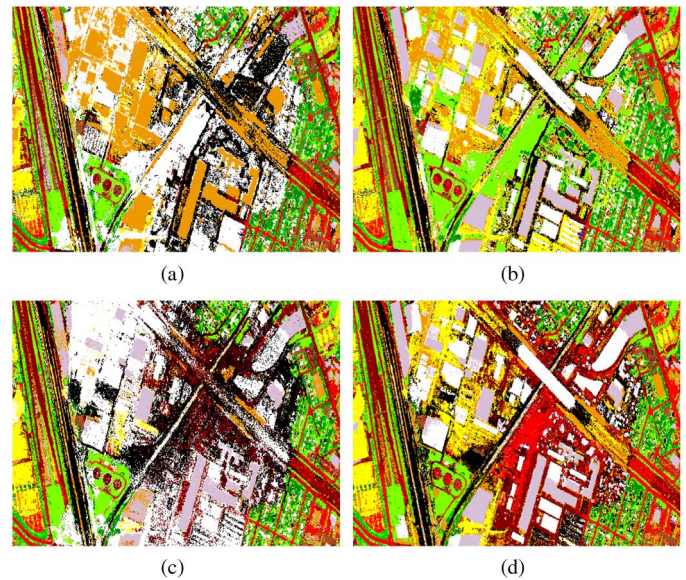


Fig. 4. Pixel based classification in the shadowed area with (a) 50 abundance features and (b) 50 abundance features and LiDAR, and (c) with 50 principal components and (d) 50 principal components and LiDAR.

case of adding it to the same number of principal components from principal component analysis (PCA). It can be observed that more fine-grained structures and more classes are detectable with the abundance feature-based approach. This may be due to the fact that the abundance features are already noise-segregated. Thus, adding LiDAR data to them provides the type of topology-related information required to discriminate corner-cases (e.g., different types of buildings or vegetation). This means abundance features can be used not only for dimensionality reduction [48], [49], but also for classification improvement [50].

When multiple models for classification are available, cross-validation is often applied. The rationale is that it is possible to assess the predictive power of different models by simply comparing them on data that was not used during the training phase. Instead of trying to find the best model, ensemble methods combine them to achieve better predictive performance than that of any model alone. As a supervised learning technique, an ensemble represents a single hypothesis, but one that is not necessarily contained within the space of the models used in the ensemble. One of the ensemble methods that have gained significant attention in recent years is the Random Forest algorithm, which is based on multiple classification tree instances [51].

The Random Forest algorithm utilizes both bagging and random attribute subset selection for achieving diversity between weak learners. As indicated by various studies (e.g., [51]–[56]), Random Forests have emerged as a powerful approach with performance similar to boosting [57], [58], SVMs [16], [59], [60], and Neural Networks [61]–[63]. Some of their advantages include low computational cost, inherent support of parallelism, accurate predictions, and the ability to handle a large number of input variables without over-fitting. In the proposed framework, the presence of shadow is detected in a pre-processing step. This information is then used to create two separate Random Forest models, one for the shadow-covered area and the other for the shadow-free area.

In addition to the attractive theoretical properties [51], Random Forest offers the advantage of feature selection capability. This is particularly useful when the training set is very small as in the Contest (approximately, only 0.4% of the total number of pixels were used for training). The reason is that as the volume of the feature space increases, the data becomes increasingly sparse in the space it occupies and this makes it difficult to achieve statistical significance for many learning methods, an aspect of the curse of dimensionality. The random forest “Out of Bag” error was used to automatically evaluate features according to their impact, resulting in 45 features selected for the shadow-free and 55 for the shadow-covered areas. The outcome of the two ensembles and their uncertainties are then synthesized based on the binary shadow index for classification.

3) *Object-Based Classification and Correction*: The unsupervised branch provides information on the object level, whereas the supervised one provides the required class label. These two streams are combined to achieve object-based classification, allowing to take the spatial context into account. This is achieved by conducting the two steps consecutively: the “object correction”, which implements a voting scheme for every object based on class uncertainties, and the “post-classification segmentation”, which performs a label reassignment on the pixel level by modeling the classification outcome as an MRF.

Let f_i denote the i th pixel of the observed scene with label ℓ_i which can take values $c \in \mathcal{C}$, where \mathcal{C} is the set of labels. The outcome of the pixel-based classification is a soft decision, meaning that the class probability distribution $p(\ell_i = c)$ is obtained for all i . Let \mathcal{O}_k denote the set of pixels in the k th object extracted in the unsupervised step. The reassignment of class labels for all objects can be expressed as

$$\ell_i^R = \operatorname{argmax}_c \sum_{f_j \in \mathcal{O}_k} p(\ell_j = c) \quad \forall \{i | f_i \in \mathcal{O}_k\} \quad (4)$$

meaning that the average class certainty needs to be maximized for every object. To prevent single-labeling of objects consisting of more than one class, (4) can be conditioned to

$$\frac{1}{N_k} \sum_{f_j \in \mathcal{O}_k} p(\ell_j = c) > p_0 \quad (5)$$

where N_k is the number of pixels in the k th object, and $(1 - p_0)$ is the average acceptable error (set to 10%, in these experiments). In particular, (5) allows objects belonging to more than one class to remain unaltered. This object correction step combined with the Hough transform is referred to as man-made structure (MMS) correction in the remaining of this section.

The object correction step previously described is applied to objects that have significant spatial extent, characteristics similar to streets or buildings, or high confidence [e.g., considering (5)] only. This conservative approach is necessary to ensure that the strict treatment of an object belonging to a single class as executed by (4) should take place only in the case of strong confidence.

Most of the pixels in the image will not be affected by the object correction methodology. For the remaining pixels, the label field resulting from the considered classifier is modeled as an MRF. With \mathbf{f} and $\boldsymbol{\ell}$ denoting the vectorized version of the label

TABLE III
PERFORMANCE COMPARISON OF PIXEL-BASED SVM CLASSIFICATION, PIXEL-BASED CLASSIFICATION USING TWO RANDOM FORESTS, MMS CORRECTION, AND POST-CLASSIFICATION SEGMENTATION

Class	SVM	2x RF	MMS Cor.	Post Seg.
Healthy grass	82.24	83.38	83.48	83.47
Stressed grass	82.99	97.74	97.56	97.56
Synthetic grass	99.60	99.60	99.80	100.00
Tree	89.87	98.30	97.63	97.63
Soil	98.56	99.24	98.58	100.00
Water	83.92	95.10	87.41	88.11
Residential	79.85	90.95	87.13	90.95
Commercial	43.11	94.11	95.06	97.44
Road	66.38	83.10	85.65	89.90
Highway	82.62	52.51	94.40	96.91
Railway	81.69	85.01	81.69	93.64
Parking 1	75.31	84.05	80.69	96.35
Parking 2	66.32	82.10	70.52	75.79
Tennis court	98.38	99.59	100.00	100.00
Running track	97.67	97.46	98.10	100.00
OA (%)	80.10	88.10	90.60	94.40
AA (%)	81.90	89.50	90.50	93.90
κ	0.784	0.871	0.898	0.940

field (as outcome of the classifier) and the true (unknown) underlying label field, a MAP approach is considered:

$$\boldsymbol{\ell}^{\text{MRF}} = \operatorname{argmax}_{\boldsymbol{\ell}} \{p(\boldsymbol{\ell})p(\mathbf{f}|\boldsymbol{\ell})\}. \quad (6)$$

The conditional probability $p(\mathbf{f}|\boldsymbol{\ell})$ can be approximated by the class probability distribution $p(\ell_i = c)$. Equation (6) can be maximized iteratively by the ICM algorithm using a standard Ising model as prior $p(\boldsymbol{\ell})$. Solving the optimization problem in (6) can effectively manage the tradeoff between the following requirements:

- 1) A pixel always has to be seen in the context of its neighborhood. Neighboring pixels tend to belong to the same class, which means $p(\boldsymbol{\ell})$ should be maximized.
- 2) Assume that an appropriate classifier has been trained properly with a discriminative set of features, the class-conditional probabilities provide the best indication of the true underlying class, which means $p(\mathbf{f}|\boldsymbol{\ell})$ should be maximized.

B. Results and Discussion

Table III illustrates the classification accuracy per class, the overall accuracy (OA), class average accuracy (AA), and the kappa coefficient (κ) for each of the following cases:

- 1) pixel-based SVM classification;
- 2) pixel-based classification using two Random Forests (one for the shadow-covered and one for the shadow-free area);
- 3) MMS correction, e.g., highway or large buildings;
- 4) post-classification segmentation.

All cases, apart from the pixel-based SVM classification, are applied consecutively on top of the previous step. It is clear that the use of two Random Forests offers a significant boost over the single SVM, since it allows for different tradeoffs of bias-variance decomposition for the shadow-covered and shadow-free areas of the image. More specifically, the Random Forest algorithm can achieve several tradeoffs through the selection of the number of features evaluated in a node split. Therefore, this flexibility allows

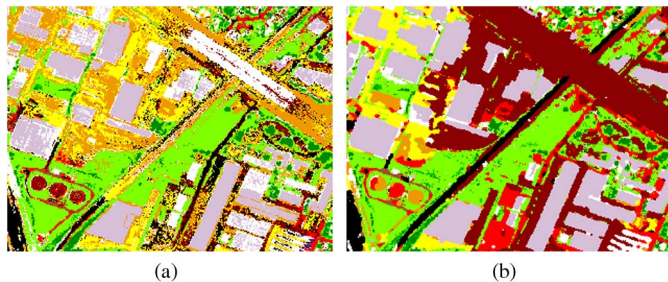


Fig. 5. Comparison of pixel-based classification with (a) Random Forests and (b) additional object-based classification over the shadowed area.

for a more fine grained decision when the model parameters can be appropriately estimated (e.g., those in the shadow-free parts of the image) and a more coarse decision, but still correct in the important parts, when parameters are more difficult to estimate (e.g., those in the shadow-covered parts of the image).

The correction of MMSs offers a dramatic increase in the case of the highway, but the enforced symmetry can also decrease slightly the accuracy of classes such as small residential buildings and parking lots. Finally, post-classification segmentation reduces the presence of outlier pixels in an otherwise homogeneous neighborhood and this improves most of the classes. It is worth mentioning that while none of the classes had 100% accuracy before the final optimization, three classes (soil, tennis court, and running track) achieved the absolute score in the last correction round.

The improvement of using object-based classification (represented in the last two columns of Table III) is depicted in Fig. 5. The improvement is evident in the areas of highway and railway (since they do not show missing parts), and large buildings (as they are classified with the right label, and not as residential pixels). Finally, Fig. 6 shows the final classification map using two random forests (one for the shadowed area and the other for the remaining image), MMS correction for highways, commercial buildings, and railways, as well as the post-classification segmentation.

V. GRAPH-BASED FEATURE FUSION OF HYPERSPECTRAL AND LIDAR DATA USING MORPHOLOGICAL FEATURES

In this section, a graph-based fusion method is proposed to couple dimensionality reduction and data fusion of spectral information (of the original HSI) and features extracted from morphological operations computed from both hyperspectral and LiDAR data together. First, morphological features are extracted from the first several principal components of the original HSI and LiDAR data. Then, a fusion graph is built where only the dimensional normalized feature points with similar spectral, spatial, and elevation characteristics are connected. Finally, the problem of multi-sensor data fusion is solved by projecting all the features into a low-dimensional subspace, on which neighborhood relationships among data points (i.e., with similar spectral, spatial, and elevation characteristics) in the original space are maintained.

A. Proposed Method

1) *Morphological Features*: Morphological features are generated using either morphological openings or closings by

reconstruction on the image, with a structural element (SE) of predefined size and shape. The morphological profile (MP) with disk SE carries information about the minimum size of objects, whereas directional MP indicates the maximum size of objects [64]–[66]. Opening operations act on bright objects (for LiDAR data, the bright regions are areas with the high elevation, such as the top of a roof) compared with their surroundings, whereas closing operations act on dark (low height in the LiDAR data) objects. Moreover, an opening operation deletes (meaning that the pixels in the object take on the value of their surrounding) bright objects that are smaller than the SE. By increasing the size of the SE and repeating the previous operation, a complete MP is built, carrying information about the size and shape of objects in the image.

The high dimensionality of hyperspectral data, in addition to redundancy within the bands, make the analysis of MPs, if extracted from each band, very challenging. To overcome this problem, FE is first used to reduce the dimensionality of these hyperspectral data, and then morphological processing is applied on each extracted feature band independently. The effect of different FE methods on extracting features from the hyperspectral data to build MPs has been discussed in several studies [38], [66]. In this paper, PCA was used to reduce the dimensionality of original hyperspectral data, and then the first few extracted PCs were used to generate the MPs, similarly as done in [38]. More specifically, in this section morphological features are generated by applying morphological openings and closings with partial reconstruction [64]–[66] on both LiDAR data and the first two PCs (representing more than 99% of the cumulative variance) of original HSI. The effect of using morphological features with partial reconstruction for classification of remote sensing data has been discussed in [64]–[66]. For disk-shaped SE, MPs with 15 openings and closings (ranging from 1 to 15 with step size increment of 1) are computed for both LiDAR data and the first two PCs of HSI. For linear structuring elements, MPs with 20 openings and closings (ranging from 5 to 100 with step size increment of 5) are constructed for both LiDAR data and the first two PCs of HSI. Figs. 7 and 8 shows the results of MP with partial reconstruction for both LiDAR data and the first PC of HSI in different scales. As the size of the SE increases in openings, it is possible for more bright objects (i.e., objects with high elevation) to disappear in the dark background of LiDAR data. On the other hand, more dark objects disappear in the closings of the first PC of HSI.

2) *Feature Dimension Normalization*: Different features may have different dimensionalities and characteristics. For example, the original HSI with 144 bands contains the spectral information of the various ground covers, the morphological features of LiDAR data with 70 bands (with 30 bands for disk-based MP and 40 bands for directional MP) carry the elevation information of the same surveyed area, and the morphological features of HSI with 140 bands present the spatial information. Before fusing these features, the input dimension needs to be normalized to reduce the computational cost and the noise throughout the given feature space. An effective way is to use Kernel PCA [67] for dimensionality reduction on each type of features separately, as it is suitable to describe higher-order complex and nonlinear distributions. The normalized dimension of each feature space can be chosen as the smallest dimension of all these features. In



Fig. 6. Final classification result using two random forests, MMS correction, and post-classification segmentation.

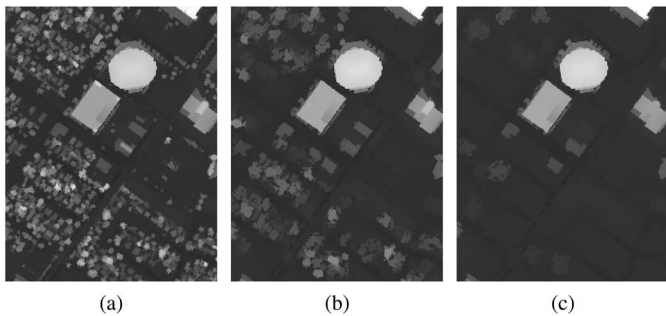


Fig. 7. Opening operations on a subset of LiDAR data with disk-shaped SEs of increasing size (1, 3, and 5).



Fig. 8. Closing operations on a subset of the first PC of the HSI with disk-shaped SEs of increasing size (1, 3, and 5).

this research, it is assumed that the dimension of each feature is already normalized to $D = 70$.

3) *Graph-Based Feature Fusion Method*: Let $\mathbf{X}^{Spe} = \{\mathbf{x}_i^{Spe}\}_{i=1}^n$, $\mathbf{X}^{Spa} = \{\mathbf{x}_i^{Spa}\}_{i=1}^n$ and $\mathbf{X}^{Ele} = \{\mathbf{x}_i^{Ele}\}_{i=1}^n$, where $\mathbf{x}_i^{Spe} \in \mathfrak{R}^D$, $\mathbf{x}_i^{Spa} \in \mathfrak{R}^D$, and $\mathbf{x}_i^{Ele} \in \mathfrak{R}^D$ denote the spectral, spatial, and elevation features, respectively, after normalization to the same dimension, respectively. Let $\mathbf{X}^{Sta} = \{\mathbf{x}_i^{Sta}\}_{i=1}^n = [\mathbf{X}^{Spe}; \mathbf{X}^{Spa}; \mathbf{X}^{Ele}]$ and $\mathbf{x}_i^{Sta} = [\mathbf{x}_i^{Spe}; \mathbf{x}_i^{Spa}; \mathbf{x}_i^{Ele}] \in \mathfrak{R}^{3D}$ denote the vector stacked by the spectral, spatial, and altitude features. Finally, let $\{\mathbf{z}_i\}_{i=1}^n$ and $\mathbf{z}_i \in \mathfrak{R}^d$ denote the fusion features in a low-dimensional feature space with $d \leq 3D$.

The goal is to find a transformation matrix $\mathbf{W} \in \mathfrak{R}^{3D \times d}$, which can couple dimensionality reduction and feature fusion in a way of $\mathbf{z}_i = \mathbf{W}^T \mathbf{x}_i$ (\mathbf{x}_i is a variable, which can set to be \mathbf{x}_i^{Sta} , \mathbf{x}_i^{Spe} , etc.). The transformation matrix \mathbf{W} should not only fuse different features in a low-dimensional feature space, but also preserve local neighborhood information and detect the manifold embedded in the original high-dimensional feature space. As

discussed in [68], a reasonable way to find the transformation matrix \mathbf{W} can be defined as follows:

$$\arg \min_{\mathbf{W} \in \mathfrak{R}^{3D \times d}} \left(\sum_{i,j=1}^n \|\mathbf{W}^T \mathbf{x}_i - \mathbf{W}^T \mathbf{x}_j\|^2 A_{ij} \right) \quad (7)$$

where the matrix \mathbf{A} is the edge of the graph $\mathbf{G} = (\mathbf{X}, \mathbf{A})$. It can be assumed that the edge (between data point \mathbf{x}_i and \mathbf{x}_j) $A_{ij} \in \{0, 1\}$; $A_{ij} = 1$ if \mathbf{x}_i and \mathbf{x}_j are ‘‘close’’ and $A_{ij} = 0$ if \mathbf{x}_i and \mathbf{x}_j are ‘‘far apart’’. The ‘‘close’’ here is defined by finding the k nearest neighbors (k NN) of the data point \mathbf{x}_i . The k NN is determined first by calculating the distance (such as the Euclidean distance) between data point \mathbf{x}_i and all the data points, then sorting the distance and determining nearest neighbors based on the k th minimum distance.

When the graph is constructed from spectral features [i.e. $\mathbf{G} = \mathbf{G}^{Spe} = (\mathbf{X}^{Spe}, \mathbf{A}^{Spe})$], the k nearest neighbors (i.e., $A_{i,j}^{Sta} = 1, j \in \{1, 2, \dots, k\}$) of the data point \mathbf{x}_i^{Spe} indicate the spectral signatures of these k NN data points \mathbf{x}_j^{Spe} , which are more similar in terms of Euclidean distance. The fusion graph $\mathbf{G}^{Fus} = (\mathbf{X}^{Sta}, \mathbf{A}^{Fus})$ is defined as follows:

$$\mathbf{A}^{Fus} = \mathbf{A}^{Spe} \odot \mathbf{A}^{Spa} \odot \mathbf{A}^{Ele} \quad (8)$$

where the operator ‘‘ \odot ’’ denotes element-wise multiplication, i.e., $A_{i,j}^{Fus} = A_{i,j}^{Spe} A_{i,j}^{Spa} A_{i,j}^{Ele}$. Note that $A_{i,j}^{Fus} = 1$ only if $A_{i,j}^{Spe} = 1$, $A_{i,j}^{Spa} = 1$, and $A_{i,j}^{Ele} = 1$. This means that the stacked data point \mathbf{x}_i^{Sta} is ‘‘close’’ to \mathbf{x}_j^{Sta} only if all individual feature points \mathbf{x}_i^{Ind} ($Ind \in \{Spe, Spa, Ele\}$) are ‘‘close’’ to \mathbf{x}_j^{Ind} . The connected data points \mathbf{x}_i^{Sta} and \mathbf{x}_j^{Sta} have similar spectral, spatial, and altitude characteristics. If any individual feature point \mathbf{x}_i^{Ind} is ‘‘far apart’’ from \mathbf{x}_j^{Ind} , then $A_{i,j}^{Fus} = 0$. For example, data points from football fields can belong to the real grass class (\mathbf{x}_i^{Sta}) or to the synthetic grass class (\mathbf{x}_j^{Sta}), resulting in similar spatial and altitude information ($\mathbf{A}_{i,j}^{Spa} = 1, \mathbf{A}_{i,j}^{Ele} = 1$), but different spectral characteristics ($\mathbf{A}_{i,j}^{Spe} = 0$). In this sense, the data points are not ‘‘close’’ (i.e., $\mathbf{A}_{i,j}^{Fus} = 0$). When using the constraint in [69] for avoiding degeneracy:

$$\mathbf{W}^T (\mathbf{X}^{Sta}) \mathbf{D}^{Fus} (\mathbf{X}^{Sta})^T \mathbf{W} = \mathbf{I} \quad (9)$$

where \mathbf{D}^{Fus} is a diagonal matrix with $D_{i,i}^{Fus} = \sum_{j=1}^n A_{i,j}^{Fus}$ and \mathbf{I} is the identity matrix, it is possible to derive the constrained solution of (7) $\mathbf{W} = (\mathbf{w}_1, \mathbf{w}_2, \dots, \mathbf{w}_r)$ which is made of r eigenvectors associated with the least r eigenvalues

TABLE IV
PERFORMANCE COMPARISON OF THE EIGHT APPROACHES AND THE PROPOSED METHOD

Class	HSI	MPs _{HSI}	MPs _{LiDAR}	MPs _{HSI} +MPs _{LiDAR}	STA	PCA	NWFE	LPP	Proposed
Healthy grass	82.15	80.25	35.61	82.43	81.10	78.63	81.29	81.10	73.31
Stressed grass	81.58	80.64	67.11	82.61	84.87	81.77	83.27	82.80	97.84
Synthetic grass	99.80	100.00	79.60	100.00	100.00	100.00	100.00	100.00	100.00
Tree	92.80	84.09	72.92	91.10	95.45	93.75	89.49	97.73	97.82
Soil	97.92	100.00	83.52	99.91	99.91	99.91	99.81	98.77	99.24
Water	95.10	95.10	66.43	100.00	95.80	95.80	95.80	95.10	99.30
Residential	76.21	87.31	76.59	80.97	86.94	84.70	86.38	84.24	88.15
Commercial	54.51	45.58	91.45	63.06	59.54	66.95	76.07	79.20	96.20
Road	78.47	91.03	59.21	91.88	90.37	83.66	93.58	91.41	86.59
Highway	60.04	60.42	64.86	64.67	65.44	57.53	62.16	61.49	76.83
Railway	79.51	87.10	88.24	93.45	99.24	97.34	98.39	92.51	92.41
Parking Lot 1	82.90	86.84	70.89	97.89	99.33	91.74	99.90	72.98	85.69
Parking Lot 2	72.63	76.49	55.09	79.30	77.19	77.54	65.26	76.00	76.49
Tennis court	100.00	100.00	100.00	100.00	100.00	100.00	100.00	100.00	100.00
Running track	97.25	100.00	14.80	100.00	98.94	100.00	100.00	97.25	99.58
No. of features	144	140	70	210	210	35	42	26	26
OA (%)	80.72	82.43	69.39	86.39	87.49	85.28	87.96	87.81	90.30
AA (%)	83.40	84.99	68.42	88.48	88.94	87.29	88.76	88.88	91.30
κ	0.792	0.810	0.668	0.853	0.864	0.840	0.869	0.868	0.895

$\lambda_1 \leq \lambda_2 \leq \dots \leq \lambda_r$ of the following generalized eigenvalue problem:

$$(\mathbf{X}^{Sta})\mathbf{L}^{Fus}(\mathbf{X}^{Sta})^T \mathbf{w} = \lambda(\mathbf{X}^{Sta})\mathbf{D}^{Fus}(\mathbf{X}^{Sta})^T \mathbf{w} \quad (10)$$

where $\mathbf{L}^{Fus} = \mathbf{D}^{Fus} - \mathbf{A}^{Fus}$ is the fusion Laplacian matrix.

B. Results and Discussion

The SVM classifier with radial basis function (RBF) [70] kernels was used in the experiments, which is known to overcome the Hughes phenomenon and perform well even with a limited number of training samples. SVM with RBF kernels has two parameters: the penalty factor C and the RBF kernel width γ . A grid-search was used on C and γ using fivefold cross-validation to find the best C within the given set $\{10^{-1}, 10^0, 10^1, 10^2, 10^3\}$ and the best γ within the given set $\{10^{-3}, 10^{-2}, 10^{-1}, 10^0, 10^1\}$. The proposed method was compared to eight alternative techniques:

- 1) using only the original HSI;
- 2) using the MPs computed on the first two PCs of original hyperspectral (MPs_{HSI});
- 3) using the MPs computed on the LiDAR data (MPs_{LiDAR});
- 4) stacking morphological features computed from both LiDAR data and the first two PCs of original HSI (MPs_{HSI} + MPs_{LiDAR}), similarly as [71];
- 5) stacking all dimensional normalized features (STA);
- 6) stacking all the features extracted by PCA from each individual features which represents more than 99% of the cumulative variance (PCA);
- 7) stacking all the features extracted by NWFE [72] from each individual feature, as [16] fused the spectral and spatial information (NWFE);
- 8) features fused by using the graph constructed by stacked features (LPP) [69]. The number of nearest neighbors is set to 20 for both LPP and the proposed method.

The classification results are quantitatively evaluated by measuring the OA, the AA, and the Kappa coefficient on the test samples. Table IV shows the accuracies obtained from the experiments, whereas the classification maps are illustrated in Fig. 9. It is shown that the objects in the shadow regions are not well classified when using hyperspectral data only or the MPs of hyperspectral

data only. Higher accuracies can be achieved in these regions using MPs derived from LiDAR data, as shown for the classes ‘‘Commercial’’ and ‘‘Highway’’ in Table IV (in fact, most test samples of these two classes are in the cloud-covered regions). The elevation features alone do not contain enough information to differentiate objects with the same elevation (e.g., grassy areas and roads on the same flat surface), as shown for the classes ‘‘Healthy Grass’’, ‘‘Road’’, and ‘‘Running Track’’ in Table IV. The overall accuracies are improved once stacking morphological features computed from both LiDAR and hyperspectral data. The proposed feature fusion method performed the best, yielding more than 10%–20% improvement compared to the base results of only using single features, and 3%–5% improvement with respect to the other fusion approaches. The techniques of (6) and (7) are similar to (5) in terms of a stacked architecture. The differences are that each individual feature is represented by different aspects, e.g., the features extracted by PCA represent most of the cumulative variance in the data, while the features extracted by NWFE represent the class discriminant. The cloud-covered regions in the original HSI are not classified well by fusing features in a stacked architecture, and the approaches (5)–(7) produced lower accuracies of ‘‘Commercial’’ than using the MPs of LiDAR only.

The spectral and spatial information of the cloud-covered regions are not related to actual land cover classes. The LiDAR data and its morphological features contain the elevation information of land cover regardless of the illumination condition. When stacking all features together, the element values of different features can be significantly unbalanced, and the information contained by different features may not be equally represented. The same problems occur when using the stacked features to build a graph in the LPP method. As shown, better accuracies can be obtained by considering the proposed method of fusion, and the cloud-covered regions of HSI are better classified.

VI. CONCLUSIONS

This paper summarized the outcome of the 2013 IEEE GRSS Data Fusion Contest, including the contributions of the two winning teams. Section IV describes a two-stream classification framework in which the hyperspectral and LiDAR data are



Fig. 9. Classification maps produced by using (a) the original hyperspectral data, (b) MPs of hyperspectral data, (c) MPs of LiDAR data, (d) the stacked features x^{Sta} , (e) the features fused by LPP on x^{Sta} , and (f) the proposed fused features.

combined by a parallel process that involves both unsupervised and supervised classification approaches, and includes a spectral unmixing step. For the Contest data set, the proposed framework produced the highest classification accuracies with a kappa coefficient of 0.940. Section V presented a methodology to fuse spectral, spatial and elevation information in the classification

process by a graph-based feature fusion approach. The morphological features with partial reconstruction, which carry the spatial and elevation information, are first generated on both the first PCs of HSI and LiDAR data. Then, a fusion graph was built where only the dimensional normalized feature points with similar spectral, spatial, and elevation characteristics are

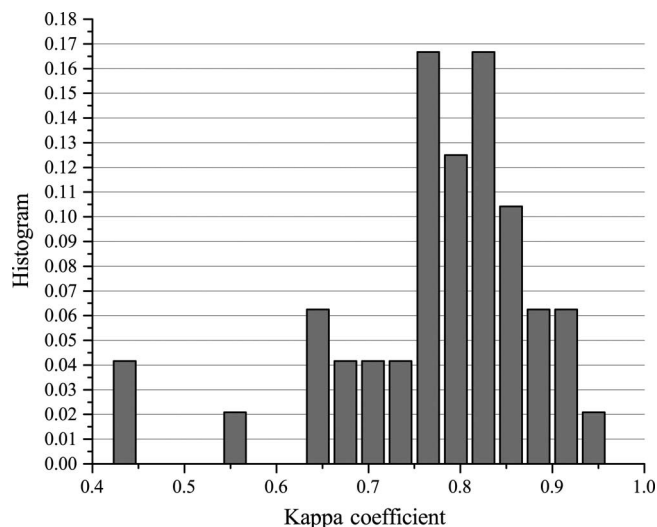


Fig. 10. Kappa distribution of the various submissions.

connected. Finally, all the features are projected into a low-dimensional space where neighborhood relationships among data points (i.e., with similar spectral, spatial, and elevation characteristics) in the high-dimensional feature space are maintained. For the Contest data set, the proposed graph-based framework yielded a classification accuracy of 0.895 in terms of Kappa coefficient.

Fig. 10 illustrates the statistics of classification accuracy provided by the various Contest submissions. As shown, about half of the classification results were between 0.700 and 0.800, and very few provided an accuracy greater than 0.900. This may be due to the presence of the large shadowed area and specific land use classes, such as “Parking Lot 1” (that included both ground level and parking garages) and “Parking Lot 2” (that actually corresponded to parked vehicles). Submissions that provided high classification performance often utilized LiDAR data in conjunction with the HSI, particularly to alleviate confusions in areas where the spectral information was not well-posed to provide a good solution (e.g., classes that had similar material compositions but different elevation profiles), and vice-versa.

In future Contests, the number of processing steps, the number of manually tuned parameters, and computational cost may be taken into consideration when evaluating the performance of algorithms.

ACKNOWLEDGMENTS

The authors and IEEE GRSS DFTC would like to express their great appreciation to the Hyperspectral Image Analysis group and the NSF Funded Center for Airborne Laser Mapping (NCALM) at the University of Houston for providing the data sets used in this study. In particular, the IEEE GRSS DFTC would like to thank X. Zhou, M. Cui, A. Singhanian, and Dr. J. Fernandez for their assistance in pre-processing the data, and assisting with related aspects of this Contest.

REFERENCES

- [1] S. Prasad and L. Bruce, “Limitations of principal component analysis for hyperspectral target recognition,” *IEEE Geosci. Remote Sens. Lett.*, vol. 5, no. 4, pp. 625–629, Oct. 2008.
- [2] S. Prasad and L. M. Bruce, “Decision fusion with confidence-based weight assignment for hyperspectral target recognition,” *IEEE Trans. Geosci. Remote Sens.*, vol. 46, no. 5, pp. 1448–1456, May 2008.
- [3] M. Chi and L. Bruzzone, “Semisupervised classification of hyperspectral images by svms optimized in the primal,” *IEEE Trans. Geosci. Remote Sens.*, vol. 45, no. 6, pp. 1870–1880, Jun. 2007.
- [4] W. Di and M. Crawford, “View generation for multiview maximum disagreement based active learning for hyperspectral image classification,” *IEEE Trans. Geosci. Remote Sens.*, vol. 50, no. 5, pp. 1942–1954, May 2012.
- [5] W. Di and M. M. Crawford, “Active learning via multi-view and local proximity co-regularization for hyperspectral image classification,” *IEEE J. Sel. Topics Signal Process.*, vol. 5, no. 3, pp. 618–628, Jun. 2011.
- [6] Y. Tarabalka, M. Fauvel, J. Chanussot, and J. Benediktsson, “SVM-and MRF-based method for accurate classification of hyperspectral images,” *IEEE Geosci. Remote Sens. Lett.*, vol. 7, no. 4, pp. 736–740, Oct. 2010.
- [7] D. Tuia, F. Ratle, F. Pacifici, M. Kanevski, and W. Emery, “Active learning methods for remote sensing image classification,” *IEEE Trans. Geosci. Remote Sens.*, vol. 47, no. 7, pp. 2218–2232, Jul. 2009.
- [8] M. Cui, S. Prasad, W. Li, and L. Bruce, “Locality preserving genetic algorithms for spatial-spectral hyperspectral image classification,” *IEEE J. Sel. Topics Appl. Earth Observ. Remote Sens.*, vol. 6, no. 3, pp. 1688–1697, Jun. 2013.
- [9] S. Serpico and L. Bruzzone, “A new search algorithm for feature selection in hyperspectral remote sensing images,” *IEEE Trans. Geosci. Remote Sens.*, vol. 39, no. 7, pp. 1360–1367, Jul. 1994.
- [10] A. Plaza, P. Martinez, J. Plaza, and R. Perez, “Dimensionality reduction and classification of hyperspectral image data using sequences of extended morphological transformations,” *IEEE Trans. Geosci. Remote Sens.*, vol. 43, no. 3, pp. 466–479, Mar. 2005.
- [11] G. Licciardi, P. R. Marpu, J. Chanussot, and J. A. Benediktsson, “Linear versus nonlinear pca for the classification of hyperspectral data based on the extended morphological profiles,” *IEEE Geosci. Remote Sens. Lett.*, vol. 9, no. 3, pp. 447–451, May 2012.
- [12] M. A. Vaughan, S. A. Young, D. M. Winker, K. A. Powell, A. H. Omar, Z. Liu, Y. Hu, and C. A. Hostetler, “Fully automated analysis of space-based lidar data: An overview of the calipso retrieval algorithms and data products,” in *Proc. Remote Sens. International Society for Optics and Photonics*, 2004, pp. 16–30.
- [13] T. Brandtberg, T. A. Warner, R. E. Landenberger, and J. B. McGraw, “Detection and analysis of individual leaf-off tree crowns in small footprint, high sampling density lidar data from the eastern deciduous forest in north America,” *Remote Sens. Environ.*, vol. 85, no. 3, pp. 290–303, 2003.
- [14] S. A. White and Y. Wang, “Utilizing DEMs derived from lidar data to analyze morphologic change in the North Carolina coastline,” *Remote Sens. Environ.*, vol. 85, no. 1, pp. 39–47, 2003.
- [15] J. Reitberger, P. Krzystek, and U. Stilla, “Analysis of full waveform lidar data for the classification of deciduous and coniferous trees,” *Int. J. Remote Sens.*, vol. 29, no. 5, pp. 1407–1431, 2008.
- [16] M. Fauvel, J. A. Benediktsson, J. Chanussot, and J. R. Sveinsson, “Spectral and spatial classification of hyperspectral data using SVMs and morphological profile,” *IEEE Trans. Geosci. Remote Sens.*, vol. 46, no. 11, pp. 3804–3814, Nov. 2008.
- [17] G. F. Hughes, “On the mean accuracy of statistical pattern recognizers,” *IEEE Trans. Inf. Theory*, vol. 14, no. 1, pp. 55–63, Jan. 1968.
- [18] H. Kalluri, S. Prasad, and L. Bruce, “Decision-level fusion of spectral reflectance and derivative information for robust hyperspectral land cover classification,” *IEEE Trans. Geosci. Remote Sens.*, vol. 48, no. 11, pp. 4047–4058, Nov. 2010.
- [19] J. Bao, M. Chi, and J. Benediktsson, “Spectral derivative features for classification of hyperspectral remote sensing images: Experimental evaluation,” *IEEE J. Sel. Topics Appl. Earth Observ. Remote Sens.*, vol. 6, no. 2, pp. 594–601, Apr. 2013.
- [20] U. G. Mangai, S. Samanta, S. Das, and P. R. Chowdhury, “A survey of decision fusion and feature fusion strategies for pattern classification,” *ETE Tech. Rev.*, vol. 27, no. 4, pp. 293–307, 2010.
- [21] L. Alparone, L. Wald, J. Chanussot, C. Thomas, P. Gamba, and L. Bruce, “Comparison of pansharpening algorithms: Outcome of the 2006 GRS-S data-fusion contest,” *IEEE Trans. Geosci. Remote Sens.*, vol. 45, no. 10, pp. 3012–3021, Oct. 2007.
- [22] F. Pacifici, F. Del Frate, W. Emery, P. Gamba, and J. Chanussot, “Urban mapping using coarse SAR and optical data: Outcome of the 2007 GRSS data fusion contest,” *IEEE Geosci. Remote Sens. Lett.*, vol. 5, no. 3, pp. 331–335, Jul. 2008.
- [23] G. Licciardi, F. Pacifici, D. Tuia, S. Prasad, T. West, F. Giacco *et al.*, “Decision fusion for the classification of hyperspectral data: Outcome of the 2008 GRS-S data fusion contest,” *IEEE Trans. Geosci. Remote Sens.*, vol. 47, no. 11, pp. 3857–3865, Nov. 2009.

- [24] N. Longbotham, F. Pacifici, T. Glenn, A. Zare, M. Volpi, D. Tuia *et al.*, "Multi-modal change detection, application to the detection of flooded areas: Outcome of the 2009-2010 data fusion contest," *IEEE J. Sel. Topics Appl. Earth Observ. Remote Sens.*, vol. 5, no. 1, pp. 331–342, Feb. 2012.
- [25] C. Berger, M. Voltersen, R. Eckardt, J. Eberle, T. Heyer, N. Salepci *et al.*, "Multi-modal and multi-temporal data fusion: Outcome of the 2012 GRSS data fusion contest," *IEEE J. Sel. Topics Appl. Earth Observ. Remote Sens.*, vol. 6, no. 3, pp. 1324–1340, Jun. 2013.
- [26] A. F. Elakshe, "Fusion of hyperspectral images and lidar-based DEMs for coastal mapping," *Optics Lasers Eng.*, vol. 46, no. 7, pp. 493–498, 2008.
- [27] A. Swatantrana, R. Dubayaha, D. Roberts, M. Hofona, and J. B. Blair, "Mapping biomass and stress in the Sierra Nevada using lidar and hyperspectral data fusion," *Remote Sens. Environ.*, vol. 115, no. 11, pp. 2917–2930, 2011.
- [28] M. Shimoni, G. Tolt, C. Perneel, and J. Ahlberg, "Detection of vehicles in shadow areas," in *Proc. 3rd Workshop Hyperspectral Image Signal Process.: Evol. Remote Sens. (WHISPERS)*, 2011, pp. 1–4.
- [29] Q. Zhang, V. P. Pauca, R. J. Plemmons, and D. D. Nikic, "Detecting objects under shadows by fusion of hyperspectral and lidar data: A physical model approach," in *Proc. 5th Workshop Hyperspectral Image Signal Process.: Evol. Remote Sens. (WHISPERS)*, 2013, pp. 1–4.
- [30] E. Simental, D. J. Ragsdale, E. Bosch, R. Dodge *et al.*, "Hyperspectral dimension reduction and elevation data for supervised image classification," in *Proc. 14th ASPRS Conf. Anchorage, AK, USA*, 2003.
- [31] D. Lemp and U. Weidner, "Improvements of roof surface classification using hyperspectral and laser scanning data," in *Proc. ISPRS Joint Conf.: 3rd Int. Symp. Remote Sens. Data Fusion Over Urban Areas (URBAN)*, 5th Int. Symp. Remote Sens. Urban Areas (URS). Tempe, AZ, USA, 2005, pp. 14–16.
- [32] J. Mundt, D. R. Streutker, and N. F. Glenn, "Mapping sagebrush distribution using fusion of hyperspectral and lidar classifications," *Photogramm. Eng. Remote Sens.*, vol. 72, no. 1, pp. 47–54, 2006.
- [33] R. Sugumaran and M. Voss, "Object-oriented classification of lidar fused hyperspectral imagery for tree species identification in an urban environment," in *Proc. Urban Remote Sens. Joint Event (JURSE)*. Paris, France, 2007, pp. 1–6.
- [34] B. Koetz, G. Sun, F. Morsdorf, K. J. Ranson, M. Kneubler, K. Itten *et al.*, "Fusion of imaging spectrometer and lidar data over combined radiative transfer models for forest canopy characterization," *Remote Sens. Environ.*, vol. 106, no. 4, pp. 449–459, 2007.
- [35] M. Dalponte, L. Bruzzone, and D. Gianelle, "Fusion of hyperspectral and lidar remote sensing data for classification of complex forest areas," *IEEE Trans. Geosci. Remote Sens.*, vol. 46, no. 5, pp. 1416–1427, May 2008.
- [36] A. Castrodad, T. Khuon, R. Rand, and G. Sapiro, "Sparse modeling for hyperspectral imagery with lidar data fusion for subpixel mapping," in *Proc. IEEE Int. Geosci. Remote Sens. Symp. (IGARSS)*, 2012, pp. 7275–7278.
- [37] L. Naidoo, M. Choa, R. Mathieu, and G. Asner, "Classification of savanna tree species, in the greater kruger national park region, by integrating hyperspectral and lidar data in a random forest data mining environment," *ISPRS J. Photogramm. Remote Sens.*, vol. 69, pp. 167–179, 2012.
- [38] M. Pedergrana, P. R. Marpu, M. D. Mura, J. A. Benediktsson, and L. Bruzzone, "Classification of remote sensing optical and lidar data using extended attribute profiles," *IEEE J. Sel. Topics Signal Process.*, vol. 6, no. 7, pp. 856–865, Nov. 2012.
- [39] M. Dalla Mura, J. A. Benediktsson, B. Waske, and L. Bruzzone, "Extended profiles with morphological attribute filters for the analysis of hyperspectral data," *Int. J. Remote Sens.*, vol. 31, no. 22, pp. 5975–5991, 2010.
- [40] M. Dalla Mura, A. Villa, J. A. Benediktsson, J. Chanussot, and L. Bruzzone, "Classification of hyperspectral images by using extended morphological attribute profiles and independent component analysis," *IEEE Geosci. Remote Sens. Lett.*, vol. 8, no. 3, pp. 542–546, May 2011.
- [41] J. Besag, "On the statistical analysis of dirty pictures," *J. R. Stat. Soc.*, vol. 48, pp. 259–302, 1986.
- [42] Q. Jackson and D. Landgrebe, "Adaptive Bayesian contextual classification based on Markov random fields," *IEEE Trans. Geosci. Remote Sens.*, vol. 40, no. 11, pp. 2454–2463, Nov. 2002.
- [43] C. Debes, J. Hahn, A. Zoubir, and M. Amin, "Target discrimination and classification in through-the-wall radar imaging," *IEEE Trans. Signal Process.*, vol. 59, no. 10, pp. 4664–4676, Oct. 2011.
- [44] C. Debes, A. Zoubir, and M. Amin, "Enhanced detection using target polarization signatures in through-the-wall radar imaging," *IEEE Trans. Geosci. Remote Sens.*, vol. 50, no. 5, pp. 1968–1979, May 2012.
- [45] R. O. Duda and P. E. Hart, "Use of the hough transformation to detect lines and curves in pictures," *Commun. ACM*, vol. 15, no. 1, pp. 11–15, Jan. 1972.
- [46] H. Ren and C.-I. Chang, "Automatic spectral target recognition in hyperspectral imagery," *IEEE Trans. Aerosp. Electron. Syst.*, vol. 39, no. 4, pp. 1232–1249, Oct. 2003.
- [47] A. Green, M. Berman, P. Switzer, and M. Craig, "A transformation for ordering multispectral data in terms of image quality with implications for noise removal," *IEEE Trans. Geosci. Remote Sens.*, vol. 26, no. 1, pp. 65–74, Jan. 1988.
- [48] B. Luo and J. Chanussot, "Hyperspectral image classification based on spectral and geometrical features," in *Proc. IEEE Int. Workshop Mach. Learn. Signal Process. (MLSP)*, 2009, pp. 1–6.
- [49] Q. Du and C.-I. Chang, "Linear mixture analysis-based compression for hyperspectral image analysis," *IEEE Trans. Geosci. Remote Sens.*, vol. 42, no. 4, pp. 875–891, Apr. 2004.
- [50] I. Dopido, A. Villa, A. Plaza, and P. Gamba, "A quantitative and comparative assessment of unmixing-based feature extraction techniques for hyperspectral image classification," *IEEE J. Sel. Topics Appl. Earth Observ. Remote Sens.*, vol. 5, no. 2, pp. 421–435, Apr. 2012.
- [51] L. Breiman, "Random forests," *Mach. Learn.*, vol. 45, no. 1, pp. 5–32, 2001.
- [52] V. Svetnik, A. Liaw, C. Tong, J. Culbertson, R. Sheridan, and B. Feuston, "Random forest: A classification and regression tool for compound classification and QSAR modeling," *J. Chem. Inf. Comput. Sci.*, vol. 43, pp. 1947–1958, 2003.
- [53] R. Diaz-Uriarte and S. A. de Andres, "Gene selection and classification of microarray data using random forest," *BMC Bioinform.*, vol. 7, no. 3, pp. 1–13, 2006.
- [54] R. Genuer, J.-M. Poggi, and C. Tuleau, "Random forests: Some methodological insights," INRIA Saclay, RR-6729, Tech. Rep., 2008, arXiv:0811.3619 [Online]. Available: <http://hal.inria.fr/inria-00340725/fr/>
- [55] R. Genuer, J.-M. Poggi, and C. Tuleau-Malot, "Variable selection using random forests," *Pattern Recognit. Lett.*, vol. 31, pp. 2225–2236, 2010.
- [56] N. Longbotham, C. Chaapel, L. Bleiler, C. Padwick, W. Emery, and F. Pacifici, "Very high resolution multiangle urban classification analysis," *IEEE Trans. Geosci. Remote Sens.*, vol. 50, no. 4, pp. 1155–1170, Apr. 2012.
- [57] R. E. Schapire, "The strength of weak learnability," *Mach. Learn.*, vol. 5, no. 2, pp. 197–227, Jul. 1990, doi: 10.1023/A:1022648800760.
- [58] Y. Freund and R. Shapire, "Experiments with a new boosting algorithm," in *Proc. 13th Int. Conf. Mach. Learn.*, I. L. Saitta, Ed. San Francisco, CA, USA, 1996, pp. 14–156.
- [59] J. Shawe-Taylor and N. Cristianini, *Kernel Methods for Pattern Analysis*. Cambridge, UK: Cambridge Univ. Press, 2004.
- [60] F. Melgani and L. Bruzzone, "Classification of hyperspectral remote sensing images with support vector machines," *IEEE Trans. Geosci. Remote Sens.*, vol. 42, no. 8, pp. 1778–1790, Aug. 2004.
- [61] J. Benediktsson, P. Swain, and O. Ersoy, "Neural network approaches versus statistical methods in classification of multisource remote sensing data," *IEEE Trans. Geosci. Remote Sens.*, vol. 28, no. 4, pp. 540–552, Jul. 1990.
- [62] F. Pacifici, M. Chini, and W. J. Emery, "A neural network approach using multi-scale textural metrics from very high resolution panchromatic imagery for urban land-use classification," *Remote Sens. Environ.*, vol. 113, no. 4, pp. 1276–1292, 2009.
- [63] G. Marchisio, F. Pacifici, and C. Padwick, "On the relative predictive value of the new spectral bands in the worldwiew-2 sensor," in *Proc. IEEE Int. Geosci. Remote Sens. Symp. (IGARSS)*, 2010, pp. 2723–2726.
- [64] W. Liao, R. Bellens, A. Pižurica, W. Philips, and Y. Pi, "Classification of hyperspectral data over urban areas using directional morphological profiles and semi-supervised feature extraction," *IEEE J. Sel. Topics Appl. Earth Observ. Remote Sens.*, vol. 5, no. 4, pp. 1177–1190, Aug. 2012.
- [65] R. Bellens, S. Gautama, L. Martinez-Fonte, W. Philips, J.-W. Chan, and F. Canters, "Improved classification of VHR images of urban areas using directional morphological profiles," *IEEE Trans. Geosci. Remote Sens.*, vol. 46, no. 10, pp. 2803–2812, Oct. 2008.
- [66] W. Liao, R. Bellens, A. Pižurica, W. Philips, and Y. Pi, "Classification of hyperspectral data over urban areas based on extended morphological profile with partial reconstruction," in *Proc. Adv. Concepts Intell. Vision Syst. (ACIVS)*. Brno, Czech Republic, 2012, pp. 278–289.
- [67] B. Scholkopf, A. J. Smola, and K. R. Muller, "Nonlinear component analysis as a kernel eigenvalue problem," *Neural Comput.*, vol. 10, pp. 1299–1319, 1998.
- [68] M. Belkin and P. Niyogi, "Laplacia eigenmaps and spectral techniques for embedding and clustering," in *Advances in Neural Information Processing Systems*, vol. 14. Cambridge, MA, USA: MIT Press, 2002, pp. 558–591.
- [69] X. F. He and P. Niyogi, "Locality preserving projections," in *Advances in Neural Information Processing Systems*, vol. 16. Cambridge, MA, USA: MIT Press, 2003, pp. 153–160.
- [70] C. C. Chang and C. J. Lin. (2001). *Libsvm: A Library for Support Vector Machines*[Online]. Available: <http://www.csie.ntu.edu.tw/~cjlin/libsvm>
- [71] M. Dalponte, L. Bruzzone, and D. Gianelle, "Tree species classification in the southern alps based on the fusion of very high geometrical resolution multispectral/hyperspectral images and lidar data," *Remote Sens. Environ.*, vol. 123, pp. 258–270, 2012.

- [72] B. C. Kuo and D. A. Landgrebe, "Nonparametric weighted feature extraction for classification," *IEEE Trans. Geosci. Remote Sens.*, vol. 42, no. 5, pp. 1096–1105, May 2004.



Christian Debes (S'07–M'09–SM'13) received the M.Sc. and Dr.-Ing. degrees (highest honors) from Technische Universität Darmstadt, Darmstadt, Germany, in 2006 and 2010, respectively.

Since 2010, he has been a Lecturer with the Department of Electrical Engineering and Information Technology, Technische Universität Darmstadt. He joined the research center of AGT International, Darmstadt, Germany, where he now holds a position as Research Architect in data analytics, in 2011. His research interests include data fusion, classification

and image processing for remote sensing applications.

Dr. Debes is a recipient of the IEEE GRSS 2013 Data Fusion "Best classification award" and has more than 25 journal and conference papers in target detection, classification and image processing. He is a Member of the editorial board of Elsevier *Digital Signal Processing*, since 2013.



Andreas Merentitis (S'06–M'10) received the B.Sc., M.Sc., and Ph.D. degrees from the Department of Informatics and Telecommunications, National Kapodistrian University of Athens (NKUA), Athens, Greece, in 2003, 2005, and 2010, respectively.

He has worked as a Senior Researcher at the NKUA and has participated in numerous European funded projects, in many cases as a Member of the proposal writing team and sub-workpackage leader of key workpackages. Since 2011, he has been working as a Senior Researcher at AGT International, Darmstadt,

Germany. He has more than 25 publications in the thematic areas of machine learning, embedded systems, distributed systems, and remote sensing, including publications in flagship conferences and journals.

Dr. Merentitis was awarded an IEEE Certificate of Appreciation as a Core Member of the team that won the first place in the "Best Classification Challenge" of the 2013 IEEE GRSS Data Fusion Contest. He is a Member of the IEEE Computer and Communication Societies, as well as the IEEE Standards Association. He holds an award from the Greek Mathematical Society and received a scholarship as one of the two highest performing M.Sc. students in his year.



Roel Heremans received the M.Sc. and Dr. degrees in elementary particle physics from the Free university Brussels (VUB), Brussels, Belgium, in 1996 and 2001, respectively.

From 2002 to 2011, he joined the Royal Military Academy, Brussels where he worked in the Signal and Image Center (SIC) on synthetic aperture processing in the field of RADAR, SONAR, and THz. In 2004, he was a Research Assistant at the NATO Underwater Research Center, La Spezia, Italy, while working on the reconstruction and motion compensation of synthetic

aperture sonar data. He developed PolInSAR features in a project for the Belgian Federal Science Policy Office (BELSPO). He was active in the field of hyperspectral image processing where he developed change detection algorithms and developed a method to determine gas pollutant concentrations above the petrochemical industry in Antwerp, Belgium. He joined AGT Germany where he has been working as a Senior Researcher on machine learning and data analytics, since 2012. He was a Scientific Evaluator of projects undertaken by the European Space Agency and Institute for Scientific Research and Innovation (IRSIB). His research interests include data fusion, classification, and change- and anomaly detection.



Jürgen Hahn (S'13) received the B.Sc. and M.Sc. degrees from Technische Universität Darmstadt, Darmstadt, Germany, in 2009 and 2011. His thesis about compressed sensing and hyperspectral imaging was awarded with the ISRA Machine Vision Prize.

Since 2011, he has been a Research Associate in the Institute of Telecommunications, Signal Processing Group, Technische Universität Darmstadt. His research interests include image processing, and classification and machine learning.



Nikolaos Frangiadakis (S'10–M'13) received the B.Sc. and M.Sc. degrees (hons.) from the Department of Informatics and Telecommunications, National Kapodistrian University of Athens (NKUA), as well as second M.Sc. and Ph.D. degrees (2011) from the University of Maryland, College Park, MD, USA.

Since 2011, he has been working as a Senior Researcher at AGT International, Darmstadt, Germany. His research interests include pervasive wireless networks, data analysis, mobility modeling, simulation, and prediction.



Tim van Kasteren received the B.Sc., M.Sc., and Ph.D. degrees from the University of Amsterdam, Amsterdam, The Netherlands, in 2003, 2006, and 2011, respectively.

He was a Post Doctoral Researcher with Bo azıcı University, Istanbul, Turkey and joined AGT in 2012 as a Senior Researcher in machine learning. His research interests include human behavior modeling, temporal probabilistic models, and data fusion.



Wenzhi Liao (S'10–M'14) received the B.S. degree in mathematics from Hainan Normal University, Haikou, China, in 2006, the Ph.D. degree in engineering from South China University of Technology, Guangdong, China, in 2012, and the Ph.D. degree in computer science engineering from Ghent University, Ghent, Belgium, in 2012.

Since 2012, he has been working as a Post Doctoral Researcher with Ghent University. His current research interests include pattern recognition, remote sensing, and image processing. In particular, his

interests include hyperspectral image restoration, mathematical morphology, and data fusion and classification.

Dr. Liao was the recipient of the 2013 IEEE GRSS Data Fusion Contest "Best Paper Challenge" Award.



Rik Bellens (M'07) received the diploma in computer science engineering in 2004, from Ghent University, Ghent, Belgium, where he is currently working toward the Ph.D. degree in the Department of Telecommunications and Information Processing.

His main research interests are pattern recognition, remote sensing, image processing, mobility and crowd behaviour.



Aleksandra Pižurica (M'03) received the diploma degree in electrical engineering from the University of Novi Sad, Serbia, in 1994, M.Sc. degree in telecommunications from the University of Belgrade, Serbia, in 1997, and the Ph.D. degree in engineering from Ghent University, Belgium, in 2002.

From 1994 to 1997, she was working as a Research and Teaching Assistant with the Department of Telecommunications, the University of Novi Sad. In 1997, she joined the Department of Telecommunications and Information Systems, Ghent University, first as a Ph.D.

student and later as a Post Doctoral Research Fellow (with the Fund for Scientific Research in Flanders *Éf* FWO Vlaanderen) and Part-Time Lecturer. Since 2011, she has been a Full-Time Professor at Ghent University in statistical image modeling. She has founded Statistical Image Modeling Lab, Ghent University and she is also leading the research unit Video and Image Content Analysis (VICA) of inter-university research Department "Future Media and Imaging" of the Flemish iMinds Institute. Her research interests include statistical image modeling, multiresolution and sparse signal representations, Bayesian estimation and applications in video analysis, remote sensing, and medical imaging.

Dr. Pižurica is currently serving as an Associate Editor for IEEE TRANSACTIONS ON IMAGE PROCESSING.



Sidharta Gautama (M'98) received the Diploma degree in electrical engineering in 1994 and the Ph.D. degree in applied sciences in 2002, both from Ghent University, Gent, Belgium.

He works at the Department of Telecommunication and Information Processing, Ghent University, first as Research Assistant and Post Doctoral Researcher, and since 2009 as a Part-Time Lecturer in computer vision. Since 2007, he heads the innovation center i-KNOW at Ghent University, which incubates the licensing and spin off activity of the research in

intelligent information processing. I-KNOW has up to now incorporated four companies and is active in the domains of environment, manufacturing, mobility, and consumer.



Wilfried Philips (S'90–M'93) was born in Aalst, Belgium, on October 19, 1966. In 1989, he received the Diploma degree in electrical engineering, and in 1993, the Ph.D. degree in applied sciences, both from Ghent University, Belgium.

From October 1989 to October 1997, he worked with the Department of Electronics and Information Systems, Ghent University, for the Flemish Fund for Scientific Research (FWO-Vlaanderen), first as a Research Assistant and later as a Post Doctoral Research Fellow. Since November 1997, he has been

with the Department of Telecommunications and Information Processing, Ghent University, where he is currently a Full-Time Professor and is heading the research group "Image Processing and Interpretation" which has recently become part of the virtual Flemish ICT research institute IBBT. Some of the recent research activities in the group include image and video restoration and analysis and the modelling of image reproduction systems. Important application areas targeted by the group include remote sensing, surveillance, and industrial inspection.



Saurabh Prasad (S'05–M'09) received the B.S. degree in electrical engineering from Jamia Millia Islamia, New Delhi, India, in 2003, the M.S. degree in electrical engineering from Old Dominion University, Norfolk, VA, USA, in 2005, and the Ph.D. degree in electrical engineering from Mississippi State University, MS, Starkville, in 2008.

He is an Assistant Professor in the Electrical and Computer Engineering Department, the University of Houston (UH), Houston, TX, USA, and leads the Hyperspectral Image Analysis Group at UH. His

group is also affiliated with the Geosensing Systems Engineering Research Center and the National Science Foundation-funded National Center for Airborne Laser Mapping. His research interests include statistical pattern recognition, adaptive signal processing, and kernel methods for medical imaging, optical, and synthetic aperture radar remote sensing. In particular, his current research work involves the use of information fusion techniques for designing robust statistical pattern classification algorithms for hyperspectral remote sensing systems operating under low-signal-to-noise-ratio, mixed pixel, and small-training-sample-size conditions.

Dr. Prasad is an active Reviewer for the IEEE TRANSACTIONS ON GEOSCIENCE AND REMOTE SENSING, the IEEE TRANSACTIONS ON IMAGE PROCESSING, the IEEE GEOSCIENCE AND REMOTE SENSING LETTERS, and the Elsevier *Pattern Recognition Letters*. He was awarded the Geosystems Research Institute Graduate Research Assistant of the Year award in May 2007, and the Office-of-Research Outstanding Graduate Student Research Award in April 2008 at Mississippi State University. In July 2008, he received the Best Student Paper Award at IEEE International Geoscience and Remote Sensing Symposium 2008 held in Boston, MA, USA. In October 2010, he received the State Pride Faculty Award at Mississippi State University for his academic and research contributions.



Qian Du (S'98–M'00–SM'05) received the Ph.D. degree in electrical engineering from University of Maryland, Baltimore, MD, USA, in 2000.

She was with the Department of Electrical Engineering and Computer Science, Texas A&M University-Kingsville, TX, USA, from 2000 to 2004. She joined the Department of Electrical and Computer Engineering, Mississippi State University, in Fall 2004, where she is currently a Full Professor. Her research interests include hyperspectral remote sensing image analysis, pattern classification, data compression, and neural networks.

Dr. Du served as Co-Chair for the Data Fusion Technical Committee of IEEE Geoscience and Remote Sensing Society in 2009–2013. She also serves as an Associate Editor for IEEE JOURNAL OF SELECTED TOPICS IN APPLIED EARTH OBSERVATIONS AND REMOTE SENSING, IEEE SIGNAL PROCESSING LETTERS, and *Journal of Applied Remote Sensing*. She received the 2010 Best Reviewer award from IEEE Geoscience and Remote Sensing Society. She is the General Chair for the 4th IEEE GRSS Workshop on Hyperspectral Image and Signal Processing: Evolution in Remote Sensing (WHISPERS) in Shanghai, China, in 2012. She is a member of SPIE, ASPRS, and ASEE.



Fabio Pacifici (S'03–M'10–SM'13) received the Ph.D. degree in geoinformation from Tor Vergata University, Rome, Italy, in 2010. He also received the Laurea Specialistica (*cum laude*) and Laurea (*cum laude*) degrees in telecommunication engineering from Tor Vergata University, in 2006 and 2003, respectively.

Since 2009, he has been with DigitalGlobe, Inc., Longmont, CO, USA, as an R&D Scientist. Between 2005 and 2009, he collaborated as Visiting Scientist with the Department of Aerospace Engineering Sciences, University of Colorado, Boulder, CO, USA. He has been involved in various remote sensing projects commissioned by the European Space Agency. His research activities include processing of remote sensing images, data fusion, feature extraction, pattern recognition, and analysis of multi-angular and multi-temporal data. His interests include classification and change detection techniques for urban remote sensing applications using very high-spatial resolution optical and/or synthetic aperture radar imagery, with special emphasis on machine learning. He has authored (or co-authored) more than 70 scientific publications including journal papers, book chapters, and peer-reviewed conference proceedings.

Dr. Pacifici is the current Editor of the IEEE GEOSCIENCE AND REMOTE SENSING ENEWSLETTER and serves as Associate Editor for the IEEE JOURNAL OF SELECTED TOPICS IN APPLIED EARTH OBSERVATIONS AND REMOTE SENSING (JSTARS). In 2011–2013, he served as a Chair of the IEEE Geoscience and Remote Sensing Society Data Fusion Technical Committee. He received the 2011 Best Reviewer Award from IEEE Geoscience and Remote Sensing Society for his service to IEEE JSTARS. He was the recipient of the Best Student Paper award at the 2009 IEEE Joint Urban Remote Sensing Event. He also ranked first at the 2007, 2008, and 2009–2010 IEEE Geoscience and Remote Sensing Society Data Fusion Contest. He currently serves as a Member of Technical Committee for the Joint Urban Event, and for the International Geoscience and Remote Sensing Symposium. He has been the Guest Editor of a special issue of the IEEE JOURNAL OF SELECTED TOPICS IN APPLIED EARTH OBSERVATIONS AND REMOTE SENSING on multi-angular remote sensing.